

Magnetic coupling in $\text{La}_{0.67}\text{Ca}_{0.33}\text{MnO}_3/\text{La}_{0.67}\text{Sr}_{0.33}\text{CoO}_3/\text{La}_{0.67}\text{Ca}_{0.33}\text{MnO}_3$ sandwiches

K. Zhao^{a,b,*}, J.F. Feng^a, Y.H. Huang^a, H. Li^c, H.K. Wong^c

^aBeijing National Laboratory for Condensed Matter Physics, Institute of Physics, Chinese Academy of Sciences, Beijing 100080, P.R. China

^bInternational Center for Material Physics, Chinese Academy of Sciences, Shenyang 110016, P.R. China

^cDepartment of Physics, The Chinese University of Hong Kong, Shatin, Hong Kong, P.R. China

Received 16 January 2004; received in revised form 12 October 2004; accepted 14 October 2004

Available online 11 November 2004

Abstract

$\text{La}_{0.67}\text{Ca}_{0.33}\text{MnO}_3$ (LCMO)/ $\text{La}_{0.67}\text{Sr}_{0.33}\text{CoO}_3$ (LSCO)/LCMO trilayer films are fabricated on single-crystal substrates NdGaO_3 (110) and the interlayer coupling are investigated. Compared with LCMO single layer, sandwiches showed the enhanced metal–insulator transition temperature of LCMO layers. The magnetoresistance is dependent on spacer thickness and the peak value dramatically decreases when LSCO layer is thick enough because of shorting by the LSCO layer. The magnetic coercivity H_C shows a nonmonotonic behavior with changing spacer layer thickness and the waist-like hysteresis indicates that there is an indirect exchange coupling between the top and bottom LCMO layers across the spacer layer.

© 2004 Elsevier B.V. All rights reserved.

PACS: 75.30.Vn; 75.60.Ej; 75.30.Et; 75.70.Ak

Keywords: Colossal magnetoresistance; Magnetic coupling; Hysteresis loop; Thin film

1. Introduction

The colossal magnetoresistance (CMR) manganite systems, $\text{RE}_{1-x}\text{A}_x\text{MnO}_3$ (RE=rare-earth and A=alkaline-earth elements), are a topic of active research because of their extraordinary electrical and magnetic properties, and their promise for future technological applications [1–3]. A prominent feature of these materials is the transition from a paramagnetic insulating state to a ferromagnetic metallic state upon lowering the temperature [4]. The double exchange theory was proposed to explain the concurrent occurrence of ferromagnetism and metallic transport [5]. The formation of the polaronic state aided by the Jahn-Teller distortion was proposed to interpret the unique magnetotransport phenomena [6]. Besides the scientific interest to investigate the elusive mechanism of CMR effect, some of attention has been focused on the technological applications of lanthanum manganites in spin-polarized tunnel junctions

[7] as well as in spin-polarized current injection devices [8]. Since the $\text{La}_{2/3}\text{R}_{1/3}\text{MnO}_3$ (R=Sr, Ca) layers are ferromagnetic (FM), their contact with antiferromagnetic (AF) perovskite layers may give rise to exchange coupling and exchange-biasing effects at the FM/AF interfaces that may alter the magnetotransport properties of the junctions. To date, only a little work has been done on the exchange coupling in manganite systems. In this paper, the manganese perovskite $\text{La}_{0.67}\text{Ca}_{0.33}\text{MnO}_3$ (LCMO)/ $\text{La}_{0.67}\text{Sr}_{0.33}\text{CoO}_3$ (LSCO)/LCMO sandwiches are investigated. A systematic study of the metal–insulator transition and coercivity is presented as a function of the spacer layer thickness.

2. Experiment procedures

Thin films were prepared by the facing-target sputtering technique on (110) NdGaO_3 (NGO) single-crystal substrates [9–12]. Ceramic LCMO and LSCO targets were sintered by standard procedure. The structure and orientation of the trilayers were checked by a Huber four-circle X-

* Corresponding author. Tel.: +86 10 82648060.

E-mail address: ainiphoto@163.com (K. Zhao).

ray diffractometer using Cu K α X-rays. The resistance as a function of temperature was measured by the standard four-probe technique with CIP (current in plane) geometry and the distance between voltage contacts was fixed at 6 mm. The magnetoresistance (MR) was examined with an applied field (H) of up to 10 kOe. The H was in the film plane and perpendicular to the current direction (also in the film plane). The MR ratios were estimated using the expression of $MR=[R(0)-R(H)]/R(0)$, where $R(H)$ and $R(0)$ are resistances with the applied field and without it, respectively. $R(0)$ was taken as the standard value because MR effects for LCMO were not saturated with an applied field of up to 10 kOe. The magnetic moment of the samples as functions of temperature and applied magnetic field was measured by utilizing a vibrating sample magnetometer. During the measurements, a magnetic field was applied parallel to the film surface. A small nonhysteretic contribution from the NGO substrate was eliminated by separately measuring its diamagnetic response. Especially the behavior of sandwiches at 230 K is described. This temperature is lower than T_{MI} (the metal–insulator transition temperature of LCMO layer) and higher than T_{MM} (the metal–metal transition temperature of LSCO layer). In our setup, there is a broad temperature range within which the LCMO ($T_{MI} \approx 240$ K) is ferromagnetic and metallic, whereas the LSCO ($T_{MM} \approx 210$ K) is paramagnetic and metallic.

3. Results and discussion

X-ray diffraction (XRD) θ – 2θ scan confirmed the epitaxial growth and high crystal quality (Fig. 1). The full width at half maximum (FWHM) of the (220) peak is

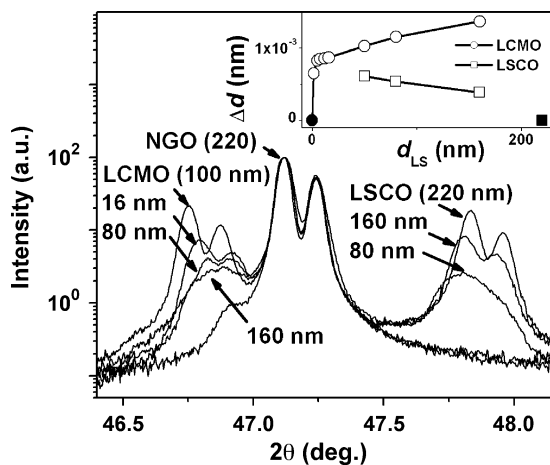


Fig. 1. X-ray diffraction patterns of LCMO (50 nm)/LSCO (d_{LS})/LCMO (50 nm) trilayers, LCMO (100 nm) and LSCO (220 nm) single layers. Numbers in the figure denote the d_{LS} values. The inset shows the variation of the out-of-plane lattice parameters of LCMO layers (open circle points) and LSCO layers (open square points). Solid square point is for LSCO (220 nm) and solid circle point is for LCMO (100 nm). Solid lines are guides for the eyes.

0.066° and 0.079° for LCMO (100 nm) and LSCO (220 nm), while it is 0.056° for the NdGaO₃ (NGO) substrate. The Φ scan of the same peak has an FWHM of 0.09° for LCMO (100 nm) and 0.06° for LSCO (220 nm), while it is 0.04° for the NGO substrate. Taking the diffraction peak of the substrate as an internal standard, the out-of-plane lattice parameters of LCMO and LSCO layers, d_{LCMO} and d_{LSCO} , can be determined accurately. As for LCMO (100 nm)/NGO and LSCO (220 nm)/NGO single-layer films, the out-of-plane lattice parameter is 0.7763 and 0.7597 nm. As shown in the inset of Fig. 1 ($\Delta d=0.7763$ nm— d_{LCMO} for LCMO layer and $d_{LSCO}=0.7597$ nm for LSCO layer), with increasing thickness of LSCO spacer layer, d_{LS} , d_{LCMO} decreased sharply from 0.7763 to 0.7755 nm and then slowly to 0.7749 nm, while d_{LSCO} decreased linearly and was close to 0.7597 nm.

For thin epitaxial film, the in-plane lattice of the sample has to match that of the substrate, and then the lattice expansion is essentially the expansion of the out-of-plane lattice parameter. LSCO has smaller lattice parameters than that of the bulk LCMO, while NGO exhibits similar lattice constants with the bulk LCMO. A tensile strain in LSCO/NGO and LSCO/LCMO and a negligibly small lattice strain in LCMO/NGO should be expected. Therefore, the out-of-plane lattice of LSCO spacer and LCMO layers should be stress and expansion, respectively, compared with that of single-layer films LSCO/NGO and LCMO/NGO. The present finding indicates that the strain-dependent effect is ruled out. Another thought is the oxygen diffusion in the interface. A lattice expansion in LSCO/NGO and LCMO/NGO due to oxygen release during the annealing is observed [13,14]. When the oxygen is migrated from the LSCO into LCMO, d_{LCMO} is shortened due to the transition of some Mn³⁺ to Mn⁴⁺, the former exhibits a larger ionic radius. Oxygen release converts some Co⁴⁺ into Co³⁺, and hence d_{LSCO} is expanded. The oxygen deficiency in LSCO is decreased with the increase of d_{LS} , therefore, d_{LSCO} draws up gradually to the out-of-plane lattice constant of LSCO (200 nm)/NGO.

Fig. 2(a) and (b) shows the temperature dependence of the resistivity (ρ) and its temperature coefficient ($d\rho/dT$) of samples. With the increase of the spacer layer thickness ($d_{LS} < 20$ nm), the resistivity curves do not show any signature of the LSCO layer and the cross points arise from the metal–insulator transition of the LCMO layers. The T_{MI} is defined as the peak point in $d\rho/dT$ curves (Fig. 2(b)). A significant change in the temperature dependence of the resistivity has been observed with the introduction of the thick LSCO spacer. The LCMO (50 nm)/LSCO (80 nm)/LCMO (50 nm) film is metallic, and the resistivity increases with temperature until ~ 210 K. At ~ 210 K, which is no different from the T_{MM} of LSCO (220 nm) film (see the inset of Fig. 2(b)), the peak value of $d\rho/dT$ occurs arising from the metal–metal transition of the LSCO layer. This kind of transition was also observed in bulk LSCO, and was ascribed to the change of magnetic order [15]. At ~ 240 K,

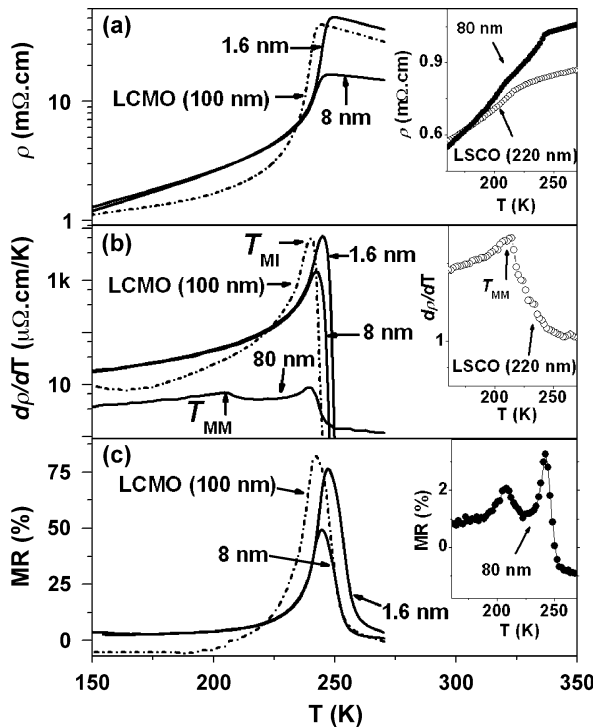


Fig. 2. (a) Resistivity (ρ), (b) differential coefficient ($d\rho/dT$) and (c) magnetoresistance (MR) as functions of temperature for LCMO (100 nm), LSCO (220 nm) and LCMO (50 nm)/LSCO (d_{LS})/LCMO (50 nm) films. Numbers in the figure denote the d_{LS} values.

another metal–metal transition occurs, leading to a flattened metallic slope. In fact, compared with the T_{MI} of LCMO (100 nm) film, this transition resulted from the metal–insulator transition of LCMO layers. So we also denote the temperature as T_{MI} .

The MR ratio (Fig. 2 (c)) is dependent on spacer thickness and the increase of LSCO layer thickness decreases the overall resistivity of the film, shifting the peak value of MR from 81% of LCMO (100 nm) to 3.33% of LCMO (50 nm)/LSCO (80 nm)/LCMO (50 nm) dramatically. The peak at ~ 205 K indicates the MR effect of the LSCO (80 nm) layer.

Fig. 3 is a summary of T_{MI} and $\rho_{230\text{ K}}$ against d_{LS} . The results show remarkable properties. In contrast to that of LCMO (100 nm) film, the T_{MI} is enhanced when the LSCO layer thickness is less than 10 nm and the peak value is 244.4 K for $d_{LS}=4.8$ nm. A relation among T_{MI} , lattice distortion and oxygen content has been established in our previous work [14], suggesting that T_{MI} decreases due to oxygen release during the annealing with the lattice expanded. The migration of oxygen from LSCO into LCMO should result in the increase of T_{MI} , which is responsible for the remarkable change in T_{MI} in part. On the other hand, the T_{MI} is close to that of the individual LCMO layer when d_{LS} is more than 100 nm, indicating that the LCMO layers are strongly coupled besides the oxygen diffusion effect, especially in the samples with thin LSCO spacer.

The enhanced T_{MI} was also found in [LCMO (10 nm)/Pr_{0.67}Ca_{0.33}MnO₃ (PCMO)]_n superlattices when PCMO thickness is less than 2 nm [10], where the exchange coupling between the LCMO layers resulted in the T_{MI} close to that of 200 nm LCMO film. In contrast, the striking discovery in T_{MI} of the present work shows that the magnetic interaction between the two LCMO layers is survived when $d_{LS}>2$ nm.

The thickness dependence of resistivity at 230 K is shown in Fig. 3. In our setup, the resistivities of LCMO (100 nm) are 2.63 m Ω cm, much larger than that of LSCO (220 nm), 0.75 m Ω cm. Thus thick LSCO layer short-circuits the LCMO layers in the sandwiches. In the parallel model of trilayers, the thick LSCO layer is the preferred conducting channel and the resistivity may be simulated by taking into account only the contribution of the LSCO layer. This effect can be seen in Fig. 3 that when $d_{LS}>50$ nm, the resistivity of sandwiches is close to that of LSCO (220 nm) film. Furthermore, an enhanced resistivity occurs and the peak value is more than 1.5 times as large as that of LCMO (100 nm). When $d_{LS}<16$ nm, the very thin LSCO spacer leads to a steep increase of its resistivity compared with LSCO (220 nm). The high resistance of the thin LSCO spacer forces the current to flow mainly through the LCMO (50 nm) top layer, and thus the resistance of trilayer is merely determined by the LCMO one. In addition, thickness effects are weak in LCMO films thicker than ~ 40 nm [16], suggesting that the enhanced resistivity resulted from some coupling between LCMO (50 nm) layers through the spacer layer.

In our previous work [9], an oscillatory resistance occurs with a period 30 nm in the series of LCMO (50 nm)/YBaCuO/LCMO (50 nm) films when the YBaCuO layer is metallic, however, here without oscillatory behavior. In general, the effects of roughness on the magnetic coupling are very important and average out the oscillatory behavior. These studies have been performed experimentally in Fe/Cr/Fe multilayers [17] and also theoretically for several FM/NM/FM multilayers [18–20]. Based on our XRD data, the lattice mismatch is 2.2% for LSCO–LCMO, larger than that

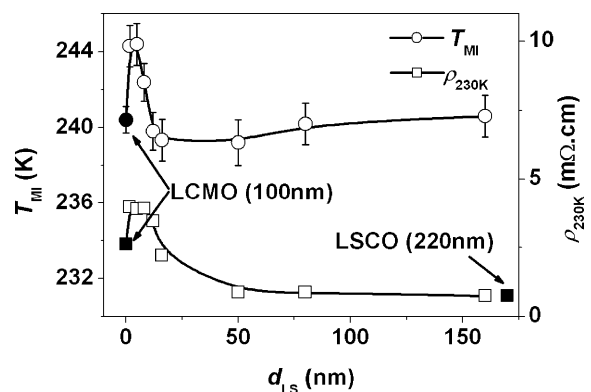


Fig. 3. T_{MI} (circle point) and $\rho_{230\text{ K}}$ (square point) as functions of LSCO layer thickness for LCMO (100 nm), LCMO (50 nm)/LSCO (d_{LS})/LCMO (50 nm) and LSCO (220 nm) films. Solid lines are guides for the eyes.

of YBaCuO–LCMO, 0.4% [21]. It is reasonable that the oscillation is partially averaged over the effects of interlayer roughness fluctuation and strain.

Compared with that for the LCMO (100 nm) film, 11%, the MR ratios for LCMO (50 nm)/LSCO/LCMO (50 nm) at 230 K (Fig. 4(a)) are enhanced when the LSCO layer thickness is less than 16 nm, suggesting LCMO/LSCO/LCMO are not simple parallel electrical circuits, but indirectly coupled between the two LCMO layers across the LSCO layer. Furthermore, when LSCO layer thickness is more than 16 nm, the metallic spacer short-circuits LCMO and diminishes the MR effect. The MR ratio drop rapidly from 11.5% at $d_{\text{LS}}=16$ nm to 2.2% at $d_{\text{LS}}=160$ nm and is close to the MR value for the LSCO (220 nm) film, 0.5%. Fig. 4(b) shows the magnetic coercivity, H_C , as a function of the spacer layer thickness for LCMO (50 nm)/LSCO/LCMO (50 nm) films at 230 K. Respectively, the magnetic coercivity is $H_{C1}=56$ Oe and $H_{C2}=62$ Oe for LCMO (100 nm) and LSCO (220 nm) films. The hysteresis loops at 230 K are also shown corresponding to the samples at the trough and peak of the H_C - d_{LS} curve (Fig. 5). The somewhat rounded rectangular shape and relatively high remnant magnetization ratio for the trilayer LCMO (50 nm)/LSCO (12 nm)/LCMO (50 nm) resembles that of a single LCMO film, suggesting that the LCMO layers in this structure are either magnetically uncoupled or coupled ferromagnetically. Different from that of LCMO film, the loop of LCMO (50 nm)/LSCO (4.8 nm)/LCMO (50 nm) shows a narrow waist, $H_C=16.2$ Oe, lower than H_{C1} and H_{C2} . Liu et al. [22] also founded the waist-like hysteresis in $\text{La}_{0.5}\text{Sr}_{0.5}\text{MnO}_3/\text{La}_{0.7}\text{Sr}_{0.3}\text{CoO}_3$ multilayers at 77 K and explained them in terms of the interlayer exchange coupling model based on the large difference in coercivity between $\text{La}_{0.5}\text{Sr}_{0.5}\text{MnO}_3$ and $\text{La}_{0.7}\text{Sr}_{0.3}\text{CoO}_3$ layers. In general, alternating hard and soft magnetic phases can lead to either a broad or a narrow waist loop. In contrast, in our system, LCMO and LSCO do not show very different magnetic hardness. It is quite reasonable that the exchange coupling between ferromagnetic LCMO layers across unferromagnetic LSCO layer

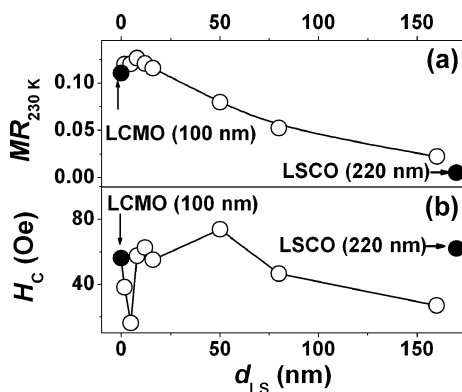


Fig. 4. $MR_{230\text{K}}$ and H_C as functions of LSCO layer thickness for LCMO (100 nm), LCMO (50 nm)/LSCO (d_{LS})/LCMO (50 nm) and LSCO (220 nm) films. Solid lines are guides for the eyes.

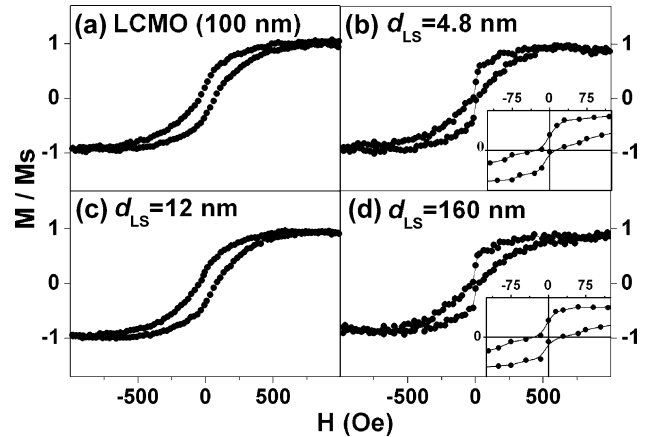


Fig. 5. Magnetic hysteresis loops of LCMO (100 nm) and LCMO (50 nm)/LSCO (d_{LS})/LCMO (50 nm) films at 230 K. The insets show the magnified loops.

bring on the nonmonotonic H_C and narrow waist-like loops. Up to $d_{\text{LS}}=160$ nm, the coupling still exists in the trilayer and results in a narrow loop with $H_C=27$ Oe.

As for ferromagnetic metal/normal metal multilayers, the main features were associated with an indirect exchange coupling between the ferromagnetic layers via the normal metal host [23–27]. An oscillatory coupling as a function of the thickness of the normal metal spacer was ubiquitously observed in several multilayered systems [28]. The prevailing experimental evidence indicates that the exchange coupling with metal spacers is short-ranged [29–31]. Very different from the usual giant magnetoresistance case, in this work, the nonmonotonic resistivity, T_{MI} , MR and H_C suggest that the magnetic interaction between the two LCMO layers still survives for thick LSCO spacer, which is also found in other manganite perovskite multilayers [9,32]. The single-step magnetization loop, measured in $\text{La}_{0.55}\text{Sr}_{0.45}\text{MnO}_3$ (30 nm)/LCMO (20 nm)/ $\text{La}_{0.55}\text{Sr}_{0.45}\text{MnO}_3$ (30 nm) trilayer, indicates that there is a ferromagnetic coupling of the $\text{La}_{0.55}\text{Sr}_{0.45}\text{MnO}_3$ layers across the LCMO spacer up to room temperature, since a two-step loop, arising from the different coercivities between LCMO and $\text{La}_{0.55}\text{Sr}_{0.45}\text{MnO}_3$ layers, should have been measured if the systems were decoupled [32]. Sirena et al. [32] attributed the long-ranged coupling to the presence of pinholes. Another possible mechanism may be related to the spin fluctuations in LCMO and LSCO layers [21]. To date, no theory has been developed to adapt to manganite perovskite multilayered system and meet such an unmonotonic behavior. It is argued that these results originate from the interlayer magnetic coupling, although a full understanding of the effects still remains open.

4. Conclusion

In summary, the perovskite LCMO/LSCO/LCMO trilayers are fabricated by a facing-target sputtering technique.

The magnetoresistance is dependent on spacer thickness and dramatically decreases when LSCO layer is thick enough because of shorting by the LSCO layer. Thin LSCO spacer resulted in the enhanced metal–insulator transition temperature of LCMO layers in sandwiches. The magnetic coercivity H_C shows a nonmonotonic behavior with changing spacer layer thickness at 230 K. A narrow waist-like hysteresis indicates that there is an indirect exchange coupling between the top and bottom LCMO layers across the spacer LSCO layer.

Acknowledgments

This work was supported by the Hong Kong Research Grant Council, the National Natural Science Foundation of China under Grant Nos. 50371102 and 10334070.

References

- [1] K. Chahara, T. Ohno, M. Kasai, Y. Kosono, Appl. Phys. Lett. 63 (1993) 1990.
- [2] R. Von Helmolt, J. Wecker, B. Holzapfel, L. Schultz, K. Samwer, Phys. Rev. Lett. 71 (1993) 2331.
- [3] S. Jin, T.H. Tiefel, M. McCromark, R.A. Fastnacht, R. Ramesh, L.H. Chen, Science 264 (1994) 413.
- [4] C.N.R. Rao, Philos. Trans. R. Soc. Lond. Ser. A: Math. Phys. Sci. 256 (1998) 23.
- [5] C. Zener, Phys. Rev. 81 (1951) 440.
- [6] A.J. Millis, P.B. Littlewood, B.I. Shraiman, Phys. Rev. Lett. 74 (1995) 514.
- [7] Y. Lu, X.W. Li, G.Q. Gong, G. Xiao, A. Gupta, P. Lecoeur, J.Z. Sun, Y.Y. Wang, V.P. Dravid, Phys. Rev., B 54 (1996) 8357.
- [8] V.A. Vasko, V.A. Larkin, P.A. Kraus, K.R. Nikolaev, D.E. Grupp, C.A. Nordman, A.M. Goldman, Phys. Rev. Lett. 78 (1997) 1134.
- [9] K. Zhao, H.K. Wong, Physica. B 349 (2004) 238.
- [10] H. Li, J.R. Sun, H.K. Wong, Appl. Phys. Lett. 80 (2002) 628.
- [11] K. Zhao, L.Z. Zhou, C.H. Leung, C.F. Yeung, C.K. Fung, H.K. Wong, J. Cryst. Growth 237–239 (2002) 608.
- [12] K. Zhao, H.K. Wong, J. Cryst. Growth 256 (2003) 283.
- [13] J.R. Sun, H.W. Yeung, H. Li, K. Zhao, H.N. Chan, H.K. Wong, J. Appl. Phys. 90 (2001) 2831.
- [14] J.R. Sun, C.F. Yeung, K. Zhao, L.Z. Zhou, C.H. Leung, H.K. Wong, B.G. Shen, Appl. Phys. Lett. 76 (2000) 1164.
- [15] M. Itoh, I. Natori, S. Kubota, K. Motoya, J. Phys. Soc. Jpn. 63 (1994) 1486.
- [16] J.R. Sun, C.F. Yeung, K. Zhao, H.K. Wong, C.M. Xiong, B.G. Shen, Physica. B 334 (2003) 310.
- [17] D.T. Pierce, J.A. Stroschio, J. Unguris, R.J. Celotta, Phys. Rev., B 49 (1994) 14564.
- [18] Y. Wang, P.M. Levy, J.L. Fry, Phys. Rev. Lett. 65 (1990) 2732.
- [19] P. Bruno, C. Chappert, Phys. Rev., B 46 (1992) 261.
- [20] M.D. Stiles, Phys. Rev., B 48 (1993) 7238.
- [21] K. Zhao, H.K. Wong, Physica C 403 (2004) 119.
- [22] J.M. Liu, Q. Huang, J. Li, C.K. Ong, Z.G. Liu, Appl. Phys., A 69 (1999) S663.
- [23] P. Grünberg, R. Scheiber, Y. Pang, M.B. Brodsky, H. Sowers, Phys. Rev. Lett. 57 (1986) 2442.
- [24] B. Heinrich, Z. Celinsky, J.F. Cochran, W.B. Muir, J. Rudd, Q.M. Zhong, A.S. Arrott, K. Myrtle, J. Kirschner, Phys. Rev. Lett. 64 (1990) 673.
- [25] S.S.P. Parkin, N. More, K.P. Roche, Phys. Rev. Lett. 64 (1990) 2304.
- [26] D.M. Edwards, J. Mathon, R.B. Muniz, M.S. Phan, Phys. Rev. Lett. 67 (1991) 493.
- [27] P. Bruno, C. Chappert, Phys. Rev. Lett. 67 (1991) 1602.
- [28] S.S.P. Parkin, Phys. Rev. Lett. 67 (1991) 3598.
- [29] J. Unguris, R.J. Cellota, D.T. Pierce, Phys. Rev. Lett. 67 (1991) 140.
- [30] J. Unguris, R.J. Cellota, D.T. Pierce, J. Magn. Magn. Mater. 127 (1993) 205.
- [31] J. Unguris, R.J. Cellota, D.T. Pierce, J. Appl. Phys. 75 (1994) 6437.
- [32] M. Sirena, N. Haberkorn, L.B. Steren, J. Guimpel, J. Appl. Phys. 93 (2003) 6177.